

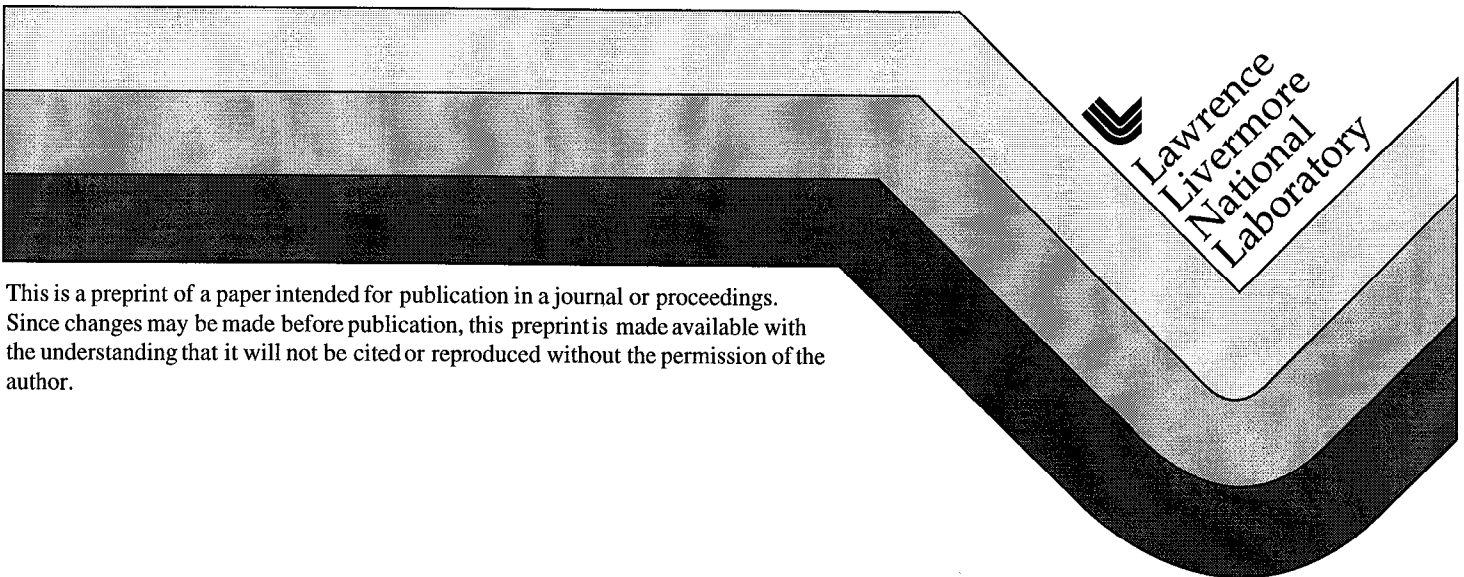
UCRL-JC-132255
PREPRINT

Linear Stability of an Accelerated Wire Array

J. H. Hammer
D. D. Ryutov

This paper was prepared for submittal to the
40th Annual Meeting of the Division of Plasma Physics
New Orleans, LA
November 16-20, 1998

October 15, 1998



This is a preprint of a paper intended for publication in a journal or proceedings.
Since changes may be made before publication, this preprint is made available with
the understanding that it will not be cited or reproduced without the permission of the
author.

DISCLAIMER

This document was prepared as an account of work sponsored by an agency of the United States Government. Neither the United States Government nor the University of California nor any of their employees, makes any warranty, express or implied, or assumes any legal liability or responsibility for the accuracy, completeness, or usefulness of any information, apparatus, product, or process disclosed, or represents that its use would not infringe privately owned rights. Reference herein to any specific commercial product, process, or service by trade name, trademark, manufacturer, or otherwise, does not necessarily constitute or imply its endorsement, recommendation, or favoring by the United States Government or the University of California. The views and opinions of authors expressed herein do not necessarily state or reflect those of the United States Government or the University of California, and shall not be used for advertising or product endorsement purposes.

LINEAR STABILITY OF AN ACCELERATED WIRE ARRAY

J.H. Hammer, D.D. Ryutov

Lawrence Livermore National Laboratory, Livermore, CA 94551

Abstract. The linear stability of an array of a large number of thin wires is considered. The wires form a cylindrical surface which is accelerated towards the axis under the action of a current excited in the array by an external source. General equations governing stability of this system are derived and a complete classification of all the modes present in such a system is presented. In agreement with an earlier analysis by Felber and Rostoker, it is shown that there exist two types of modes: medial modes, in which the wires experience deformation in the rz plane, and lateral modes, in which only a purely azimuthal deformation is present. For a given axial wave number k , the maximum growth rate for medial perturbations corresponds to a mode in which all the wires move "in phase" (an analog of an axisymmetric mode for a continuous cylindrical shell), whereas for the lateral perturbations the maximum growth rate corresponds to the opposite displacements of the neighboring wires. Numerical analysis of a dispersion relation for a broad range of modes is presented. Some limiting cases are discussed. In particular, it is shown that a traditional $k^{1/2}$ scaling holds until surprisingly high wave numbers, even exceeding the inverse inter-wire distance. In the limit of long-wavelength perturbations, a model of a continuous shell becomes valid; the presence of the wires manifests itself in this model by a strong anisotropy of electrical conductivity, high along the wires and vanishing across the wires.

The resulting modes differ considerably from the modes of a thin perfectly conducting shell. In particular, a new mode of “zonal flows” is identified.

PACS 52.55.Ez, 52.35.Py

I. INTRODUCTION

Remarkable progress has been made in recent years in experiments on Z-pinch implosions of cylindrical wire arrays [1-3]. A typical geometry for such experiments is shown in Fig. 1a. A cylindrical shell is initially made of hundreds of individual fine wires (which later in the pulse may merge together). An axial current reaching tens of megamperes is driven through the shell by the external power source. Under the action of the $\mathbf{J} \times \mathbf{B}$ force the shell is accelerated towards the axis and, after the run-in phase, collapses on axis. The pinch kinetic energy is thermalized and converted to an intense pulse of short-wavelength radiation. The radiation pulse-width is determined by the quality of the implosion, which to great extent depends on the development of instabilities of the imploding shell.

It is commonly recognized that the most detrimental instability of the imploding shell is similar to the Rayleigh-Taylor instability of two superposed fluids in the gravitational field [4]. In a co-moving frame, the shell may be thought of as a thin slab of gravitating fluid resting on another, massless fluid (the magnetic field). Although there are similarities with the usual Rayleigh-Taylor instability, there are also considerable differences caused by the differences in the structure of the stress tensor of the ordinary fluid (isotropic) and Maxwell stress tensor of the magnetic field. Because of this, the term “magnetic Rayleigh-Taylor instability” is sometimes used to make a distinction with respect to the “ordinary” instability. First assessments of the magnetic Rayleigh-Taylor instability trace back to the 1960’s [5]. More recently, in conjunction with progress in the area of fast

Z pinches, many tens of publications devoted to analytical and numerical studies of this instability have appeared (see, e.g., [6-8] and references therein).

One part of the problem that has received insufficient attention is the stability of the early stage of the implosion, before merging of the wires occurs. The wires are initially very thin and well separated from each other, making them well defined entities. In a typical experiment at the Z facility [2], the initial diameter of the tungsten wire-array is 4 cm, the number of the wires is 240, and the diameter of an individual wire is $7.5 \mu\text{m}$. In other words, the inter-wire distance a is approximately 60 times greater than the wire diameter $2r_w$. The distance D to a return-current conductor (Fig. 1) is typically a few millimeters, much greater than the interwire distance. Very early in the pulse, the wires are melted; for this reason, one can neglect the effect of elastic forces on the motion of the wires.

We will consider perturbations with a length-scale in the axial direction much greater than the diameter of an individual wire r_w . In this case, one can essentially neglect the structure of each wire and characterize it by the mass per unit length and the shape of the curve representing the wire (there is a caveat here: the effect of a self magnetic field on the wire motion logarithmically depends on the wire radius; we will take this effect into account at the appropriate point). Such an approach can be called a “thin wire model”. In the past, this model was employed in the papers by Felber and Rostoker [9], and Samokhin [10]. The first paper was concerned with oscillations and instabilities of a small number of wires, and low modes of oscillation. In the second paper, the author considered an arbitrary number of wires, but only for the modes of mutual translation, which keep the wires straight and parallel to the axis. Later, a similar study was carried out by DeGroot and M. Liberman [11]. In our study, we will concentrate on the case of a large number of wires in the array and will cover all modes possible in the thin-wire model.

In some of the recent experimental studies it was found that, early in the pulse, some small fraction of the wire material forms a hot “halo” around cold wire cores where

most of the mass resides (e.g., [12-14]). The halo may intercept a considerable fraction of the current in the case of an isolated wire. Since the halo expands rapidly to distances of order the interwire gap, this brings into question the utility of the thin wire model. For a realistic wire array, however, there is a large collective azimuthal magnetic field outside of the array and small collective field within the array. In the presence of the collective field, the behavior is expected to be quite different than in the single wire case. The $\mathbf{J} \times \mathbf{B}$ forces in the collective field blow the halo plasma radially inward past the wire cores, exposing the cores to the applied electric field and thereby transferring much of the current to the cores. Recent 2D MHD simulations show that the array retains an azimuthal structure with relatively cool, current carrying plasma cores well into the implosion [15]. Regardless of the detailed structure of the halo/core wire array plasma, we believe that the thin-wire model provides valuable insight into the effects of azimuthal nonuniformity on pinch instability.

Of prime concern in the implosion are modes with high growth-rates. These modes correspond to the perturbations whose axial and azimuthal extent is much less than the radius of the wire array. For such modes, one can replace the cylindrical wire array by an infinite curtain of wires. This is illustrated in Fig. 1b where the coordinate system is also introduced. Unless stated otherwise, we will use this approximation.

The further organization of the paper is as follows: in Sec. II, we consider the formulation of the problem and basic equations. The periodicity of the wire array allows one to find a universal relationship between displacements of the wires in the eigenmode. In Sec. III, we evaluate the perturbation of the magnetic field produced by an individual deformed wire, perform a summation over the wires and arrive at the equation for linear oscillations. In Sec. IV we derive and analyse dispersion relations for medial and lateral eigenmodes. We discuss some limiting cases and, in particular, a long-wavelength case which, as it turns out, differs significantly from the case of a continuous conducting shell [5]. For perturbations with azimuthal and axial scale-length exceeding the distance D between the wire array and return-current conductor, the presence of this conductor appears

to be important and causes a stabilizing effect. In section V we present the summary and discuss possible generalizations. In the Appendix we derive dispersion relations for long-wavelength modes based on a model of a quasicontinuous shell.

II. BASIC EQUATIONS

The geometry of the planar problem is illustrated by Fig. 1b. The wires intersect the $z=0$ plane in the points $x=0, y=na$, where n is an integer, $n=0, \pm 1, \dots$. The current per wire is I_w , the vertical current per unit length of the array is $J=I_w/a$. At distances of the order of a the magnetic field of the wire array becomes uniform; this uniform field has only a y component, equal to $-\mu_0 J/2$ (at $x<0$), and $\mu_0 J/2$ (at $x>0$) where μ_0 is the magnetic permeability of the vacuum. Superimposed on this field is the magnetic field B_{ret} of the return current conductor, which has only the y component [equal to $\mu_0 J/2$ (at $x<-D$) and $-\mu_0 J/2$ (at $x>-D$)]. As a result, the smoothed magnetic field B_y is present only in the gap between the wire array and the return current conductor. It is equal to:

$$B_y = B \equiv \mu_0 J \quad (1)$$

These considerations are necessary only in the case of the planar model. For a cylindrical array of Fig. 1a, it is obvious from the outset that the unperturbed magnetic field is present only in the gap between the array and the return current conductor. The magnetic field in the gap and near the wire array is equal to (1).

In the planar model, the x component of the force acting on a wire from the other wires in the unperturbed state is, obviously, zero (because of the symmetry of the problem). Therefore, the acceleration of the array in the direction $x>0$ occurs under the action of the magnetic field created by the return-current conductor, namely, by the magnetic field

$$B_{ret} = -\mu_0 J/2 \quad (2)$$

The force acting per unit length of a single wire is equal to

$$f_x = -I_w B/2 = \mu_0 I_w J/2 = a \mu_0 J^2/2 = aB^2/2\mu_0 \quad (3)$$

and causes the acceleration of the array:

$$\ddot{x} = f_x / \hat{m}. \quad (4)$$

where \hat{m} is a mass of a unit length of an individual wire. In the frame co-moving with the array in the x direction, the array is under the action of the two forces, the force f_x , and the effective gravity force acting in the negative direction of the axis x . The effective gravity acceleration is

$$g_x \equiv g = I_w B/2 \hat{m} = -\mu_0 I_w J/2 \hat{m} = -\mu_0 a J^2/2 \hat{m} = -aB^2/2\mu_0 \hat{m}. \quad (5)$$

We will use these alternative representations for g in our further analysis.

In the co-moving frame, the unperturbed wires are at rest. We impose small perturbations on this initial state and analyze their evolution in the linear approximation. As is known from the analyses of the Rayleigh-Taylor instability, the growth rate increases with decreasing length-scale. For this reason, we will concentrate on the analysis of perturbations with length-scales much shorter than the gap, D , between the wire array and return current conductor. In this case, perturbations of the magnetic field by the perturbed image currents are exponentially small and for now will be neglected (in Sec. V we discuss the case of larger wavelengths, where this effect is essential).

Consider a perturbation of the line representing an initially straight wire (Fig. 2). Following an approach first proposed by Ott in the analysis of a stability of a thin continuous sheet, we use the Lagrangian description, where the displacement of a certain point of the wire having the initial coordinate z is characterized by the displacement vector $\xi_n(z, t)$. The subscript n refers to a particular wire. We consider two points on the initially straight wire separated by a small distance, Δz . The mass of the corresponding segment of

the wire is $\Delta m = \hat{m} \Delta z$ and remains constant in the course of the subsequent motions. At time t , the ends of the segment Δz will be situated at the points $e_z z + \xi_n(z, t)$, and $e_z z + \xi_n(z, t) + (e_z + \partial \xi_n(z, t) / \partial z) \Delta z$, respectively. In other words, the length of the initial segment becomes $(1 + \partial \xi_{nz}(z, t) / \partial z) \Delta z$ and changes by

$$\Delta z \partial \xi_{nz}(z, t) / \partial z \quad (6)$$

compared to its initial length (we retain only corrections of the first order).

The equation of motion of the wire has the form:

$$\Delta m \ddot{\xi} = \delta \mathbf{f} \quad (7)$$

where $\delta \mathbf{f}$ is a perturbation of the force acting on the chosen element of the wire. To simplify notation, we skip here and in a few further equations the subscript “ n ”. Because the mass of the Lagrangian element does not change, the perturbation of the gravity force is zero. We therefore need to find only the perturbation of the magnetic force. It consists of several contributions:

$$\delta \mathbf{f} = \Delta z \left(\frac{\partial \xi_z}{\partial z} \mathbf{I}_w \times \mathbf{B}_{\text{ret}} + \delta \mathbf{I}_w \times \mathbf{B}_{\text{ret}} + \mathbf{I}_w \times \delta \mathbf{B}_L + \delta \hat{\mathbf{f}}_{\text{self}} \right) \quad (8)$$

The first term represents the variation of the force acting on a certain Lagrangian element of the wire; this variation is caused by the change of the length of the element (Eq. (6)). The second term describes the variation of the force caused by the variation of the direction of the current:

$$\delta \mathbf{I}_w = I_w \frac{\partial \xi_{\perp}}{\partial z} \quad (9)$$

For the reasons that we describe shortly, we assume that the magnitude of the current in the wire does not change. Note that the contribution to the first two terms in the r.h.s. of Eq. (8) comes only from the interaction with the magnetic field of the return current conductor (2) (because the unperturbed magnetic field of the wire array in the unperturbed location of

the wire is zero). The third term arises from the interaction of the unperturbed current with the magnetic field perturbation in the location of the Lagrangian element, $\delta\mathbf{B}_L$. For $\delta\mathbf{B}_L$ one has:

$$\delta\mathbf{B}_L = \delta\mathbf{B} + \xi \cdot \nabla\mathbf{B} \quad (10)$$

where $\delta\mathbf{B}$ is the perturbation of the magnetic field in the initial location of the Lagrangian element (at $\xi=0$) by all the wires except the one whose displacement we study. Finally, the fourth term in the r.h.s. of Eq. (8) describes the force acting on the wire because of the magnetic field perturbation produced by deforming this wire itself. The reason for singling out this term is that, in evaluating it, one has to take into account the finite radius of the wire (which, as we will see, enters expression for $\hat{\delta}\mathbf{f}_{self}$ only logarithmically).

The r.h.s. of Eq. (8) is a linear functional of the displacements ξ_n of the wires. As the system is assumed to be uniform in the z direction, one can apply a Fourier transform over this coordinate, and seek a solution $\propto \exp(ikz)$. After having done that, one arrives at the set of $3N$ ordinary second-order differential equations (in time) for the functions $\xi_{nx}(t)$, $\xi_{ny}(t)$, and $\xi_{nz}(t)$ (N is the total number of the wires in the array). As the time does not explicitly enter this set of equations, we will seek the solution proportional to $\exp(\gamma t)$; the positive real part of γ corresponds to the instability. A solution varying as $\exp(\gamma t)$ is only formally valid for time-invariant coefficients in the equations, however the analysis remains valid if the coefficients vary on a time scale $\tau \gg \gamma^{-1}$, and the time dependence of the solution becomes approximately $\exp\left(\int \gamma dt\right)$. We expect this approximation to be well satisfied for the rapidly growing modes under consideration.

For perturbations having an $\exp(ikz)$ dependence on z , with k nonzero, the magnitude of the current in each wire remains unperturbed. This can easily be seen since a perturbed current magnitude, δI_z , must be independent of z by current continuity and a $\delta I_z \times B_{ret}$ force independent of z would appear in eq.(8), violating the assumed $\exp(ikz)$ variation. Alternatively, a z -independent current perturbation would require a net z -averaged axial electric field, which is inconsistent with $\exp(ikz)$ eigenfunctions. The special case, $k = 0$, was treated by Samokhin and will not be discussed further here.

The eigen-solutions of the set of equations possess a general property that stems from the periodicity of the system in the azimuthal (y) direction: one can show that

$$\xi_{n+1} = \exp(2\pi im/N) \xi_n, \quad m = 0, \pm 1, \dots, \pm \frac{N-2}{2}, \frac{N}{2}. \quad (11)$$

where N is the number of the wires in the wire array; we assume that N is an even number. Each value of m corresponds to some eigenfunction of the aforementioned set of the dynamic equations.

To prove Eq. (11), one can use the following arguments (essentially identical to those used in the derivation of Bloch-wave solutions in the problem of eigenfunctions in crystals, e.g.[16]): let ξ_n be some eigenmode of the problem, with a certain dependence of ξ_n over n . Let us turn the whole array by an angle $2\pi/N$. This transformation maps the array into itself, whereas the eigenfunction becomes the one with $\xi_{n+1} \rightarrow \xi_n$. The new eigenfunction, obviously, corresponds to the same eigenvalue as the old one and can therefore differ from the old one only by a constant multiplier,

$$\xi_{n+1} = C \xi_n \quad (12)$$

Having performed the same transformation N times, we return to the initial eigenfunction. Therefore, the coefficient C in (12) should be a solution of the equation

$$C^N=1 \quad (13)$$

This equation has N solutions, corresponding to various eigenfunctions:

$$C_m = \exp(2\pi im/N), \quad m = 0, \pm 1, \dots, \pm \frac{N-2}{2}, \frac{N}{2}. \quad (14)$$

In the problem under consideration, this result was first used in [9, 10]. We will find that the eigenvalues are degenerate for $m \rightarrow -m$, so that alternate representations of the eigenfunctions consisting of linear combinations of $\pm m$ eigenfunctions are also possible.

We are interested in the behavior of the array consisting of a large number of wires

$$N \gg 1 \quad (15)$$

In this case, small mode numbers m correspond to smooth azimuthal perturbations. In particular, the $m=1$ mode corresponds to a kink perturbation of a cylindrical conducting shell. In these modes the neighboring wires experience almost the same displacements. It goes without saying that the mode $m=0$ corresponds to an axisymmetric perturbation, where all the wires experience the same displacement (at a given z). We will discuss these issues in more detail in the next section.

The mode numbers with large m correspond to the perturbations in which the neighboring wires experience considerably different displacements. In particular, for $m=N/2$, one obtains a mode in which the neighboring wires experience oppositely directed displacements (Fig. 3).

In Sec. 3 we also show that the last term in the r.h.s. of Eq. (8) can be presented as:

$$\hat{\delta \mathbf{f}}_{self} = -k^2 \Lambda(k) (\mu_0 / 4\pi) I_w^2 \xi_{\perp} \quad (16)$$

where $\Lambda(k)$ is a function weakly (logarithmically) dependent on k (see Sec. III for the derivation).

With these observations made, it is clear that the three components of Eq. (8) can be written as:

$$\gamma^2 \hat{m} \xi_{nz} = \frac{i}{2} k \xi_{nz} I_w B - I_w \delta B_y + k^2 \Lambda(k) (\mu_0 / 4\pi) I_w^2 \xi_{nz}, \quad (17)$$

$$\gamma^2 \hat{m} \xi_{ny} = I_w \delta B_x + k^2 \Lambda(k) (\mu_0 / 4\pi) I_w^2 \xi_{ny}, \quad (18)$$

$$\gamma^2 \hat{m} \xi_{nz} = -\frac{i}{2} k \xi_{nz} I_w B; \quad (19)$$

the definition of \hat{m} is given after Eq. (4). As will be shown in Sec. III, the y component of the wire displacement does not perturb the y -component of the magnetic field in the plane $x=0$, whereas the x -component of the displacement does not perturb the y component of the magnetic field. This means that δB_y (δB_x) in this set of equations contain only ξ_x (ξ_y). This in turn means that, in the system under consideration, there exist two separate modes. The first, where only the y component of the displacement is non-zero, can be called a “lateral” mode (Eq. (18)), i.e., displacements lie within the plane of the wire array. The second mode, where only the x - and z -components of ξ_n are non-zero, can be called a “medial” mode (Eqs. (17) and (19)) since the perturbations are directed alternately toward and away from the array plane. This observation was first made by Felber and Rostoker [9]. The structure of several lateral modes is shown in Fig. 3.

III. PERTURBATION OF THE MAGNETIC FIELD

A. Perturbation from an individual wire

Consider an initially straight wire that is directed along the z axis and intersects the (xy) plane in the point $x=0, y=0$. Let the wire be deformed in the xz plane according to equation

$$\xi_x = \xi \exp(ikz). \quad (20)$$

As we are solving a linear problem, the perturbation in the yz plane can be treated separately. The new current pattern can be presented as a set of infinitesimal closed current loops, plus the unperturbed current (Fig. 4). The perturbation of the magnetic field is created by current loops which are equivalent to magnetic dipoles oriented in the y direction and having a dipole strength (for a segment of a length dz):

$$dM_y = -(\mu_0/4\pi)I_w \xi_x dz \quad (21)$$

The magnetostatic potential ψ created by this set of the magnetic dipoles is (see [17]):

$$\psi = \frac{\mu_0 I_w \xi}{4\pi} \int_{-\infty}^{+\infty} \frac{y \exp(ikz') dz'}{[x^2 + y^2 + (z' - z)^2]^{3/2}} = \frac{\mu_0 I_w \xi_x}{4\pi} \int_{-\infty}^{+\infty} \frac{y \exp(ikz') dz'}{[x^2 + y^2 + z'^2]^{3/2}} \quad (22)$$

It is clear from this expression that $\delta B_x = -\partial\psi/\partial x$ is indeed zero in the $x=0$ plane, in agreement with the statement made in Sec. II. The absence of the perturbation of the y component of the magnetic field by the y component of the displacement can be shown analogously.

In evaluating the integral (22) and similar integrals, we will use the results of Bessel function theory (see [18], Sec. 7.12):

$$\int_{-\infty}^{+\infty} \frac{\exp(ikz') dz'}{[r^2 + z'^2]^{\ell+1/2}} = 2\sqrt{\pi} \left(\frac{k}{2r}\right)^\ell \frac{K_\ell(kr)}{\Gamma\left(\ell + \frac{1}{2}\right)} \quad (23)$$

where K_ℓ are McDonald's functions, and Γ is a gamma-function ($\Gamma(1/2)=\pi^{1/2}$; $\Gamma(3/2)=\pi^{1/2}/2$; $\Gamma(5/2)=3\pi^{1/2}/4$, etc.). The perturbation of the y component of the magnetic field in the $x=0$ plane is:

$$\delta B_y = \frac{\mu_0 I_w \xi_x}{2\pi} \cdot \left(\frac{k}{y}\right) [K_1(ky) - kyK_2(ky)] \quad (24)$$

Using the identities of the Bessel function theory [18, Sec. 7.11], one can represent Eq. (24) also in a more compact form:

$$\delta B_y = \frac{\mu_0 I_w \xi_x}{2\pi} \cdot k^2 K_1'(ky) \quad (24')$$

where prime means differentiation over the whole argument.

Analogously, perturbation of the x component in the $x=0$ plane is:

$$\delta B_x = -\frac{\mu_0 I_w \xi_y}{2\pi} \cdot \left(\frac{k}{y}\right) K_1(ky) \quad (25)$$

If we need to find the perturbed field created at the origin by the wire situated at $y=na$, the argument y in expressions (24), (25) should be replaced by $-na$, and ξ by ξ_n .

B. Perturbation of the magnetic field produced by the whole array

In this section we evaluate the perturbation of the magnetic field in the location of some particular wire, say, the wire situated in the origin. The choice of the wire is

arbitrary, as all the displacements in the eigenmode are related to each other by Eq. (11).

For our specific choice of the wire, one has

$$\xi_n = \xi_0 \exp\left(\frac{2\pi m n i}{N}\right), \quad n = \pm 1, \pm 2, \pm 3, .. \quad (26)$$

where m , as has been mentioned in Sec. 2, characterizes the azimuthal mode structure.

With these observations made, one immediately obtains the following expressions for the magnetic field perturbations in the location of the “zeroth” wire:

$$\delta B_x = -\frac{\mu_0 I_w k \xi_{y0}}{\pi a} \cdot \sum_{n=1}^{\infty} \cos\left(\frac{2\pi m n}{N}\right) \frac{K_1(kna)}{n} \quad (27)$$

$$\delta B_y = \frac{\mu_0 I_w k^2 \xi_{x0}}{\pi a} \cdot \sum_{n=1}^{\infty} \cos\left(\frac{2\pi m n}{N}\right) K_1'(kna) \quad (28)$$

We extend summations over n to the infinity, because the sums are rapidly converging.

The last step required to obtain a closed set of equations, is to find the “convective” term in Eq. (10). This term contains spatial derivatives of the unperturbed magnetic field at the position of the zeroth wire ($x=y=0$). Here we mean the field created by all the wires but the “zeroth” one. At $x=y=0$, one has:

$$\frac{\partial B_x}{\partial x} = \frac{\partial B_y}{\partial y} = 0; \quad \frac{\partial B_x}{\partial y} = \frac{\partial B_y}{\partial x} = \frac{\mu_0 I_w}{\pi a^2} \sum_{n=1}^{\infty} \frac{1}{n^2} = \frac{\pi \mu_0 I_w}{6a^2} \quad (29)$$

One, therefore, obtains the following expression for $\delta \mathbf{B}_L$:

$$\begin{aligned} \delta B_{xL} &= \delta B_x + \frac{\pi \mu_0 I_w}{6a^2} \xi_{0y} \\ \delta B_{yL} &= \delta B_y + \frac{\pi \mu_0 I_w}{6a^2} \xi_{0x} \end{aligned} \quad (30)$$

where δB_x and δB_y are determined by Eqs. (27), (28).

C. Evaluation of the force δf_{self}

To evaluate δf_{self} , we have to take into account the magnetic interaction between the elements of the current within a single wire. We split the wire into current filaments with infinitesimal cross-sections (Fig. 5). Each of them is bent in the x direction according to Eq. (20). Consider two such filaments with the infinitesimal cross-sectional areas dA_1 and dA_2 carrying the currents dI_1 and dI_2 . The x component of the force acting per unit length of the filament 1 from the side of the filament 2 is

$$df_{xself} = dI_1 d\delta B_{y12} \quad (31)$$

where δB_{y12} is the magnetic field created by filament 2 in the location of filament 1. The magnetic field perturbation can be found from Eq.(22) and has the form:

$$d\delta B_{y12} = C_{12} dI_2; \quad C_{12} = -\frac{\mu_0 \xi}{4\pi} \int_{-\infty}^{+\infty} \frac{\left[1 - \frac{3(y_1 - y_2)^2}{r_{12}^2 + z'^2}\right] \exp(ikz') dz'}{\left[r_{12}^2 + z'^2\right]^{3/2}} =$$

$$-\frac{\mu_0 \xi k}{2\pi r_{12}} \left[K_1(kr_{12}) - \frac{k(y_1 - y_2)^2}{r_{12}} K_2(kr_{12}) \right], \quad r_{12} = [(x_1 - x_2)^2 + (y_1 - y_2)^2]^{1/2} \quad (32)$$

The net force is equal to

$$f_{xself} = \int C_{12} dI_1 dI_2 = \int C_{12} j(r_1) j(r_2) dA_1 dA_2 \quad (33)$$

If in this expression one changes the place of the integration variables x and y , the result, obviously, does not change. On the other hand, this change of places causes replacement of $(y_1 - y_2)^2$ by $(x_1 - x_2)^2$ in front of the function K_2 in (32). This means that in the expression

for C_{12} that enters (33) one can replace $(y_1 - y_2)^2$ by $[(x_1 - x_2)^2 + (y_1 - y_2)^2]/2 = r_{12}^2/2$. Using the identity ([18], Sec. 7.11):

$$K_1(z) - \frac{z}{2} K_2(z) = -\frac{z}{2} K_0(z) \quad (34)$$

one arrives at the following simple expression for δf_{self} :

$$\delta f_{xself} = -\frac{\mu_0 \xi_x k^2}{4\pi} \int K_0(kr_{12}) j(r_1) j(r_2) dA_1 dA_2 \quad (35)$$

We perform the further calculations for a uniform distribution of the current over the cross-section of the wire. Instead of evaluating δf_{self} , we evaluate an equivalent quantity

Λ defined according to (16). One has:

$$\Lambda = \frac{2}{\pi} \int_0^1 \rho_1 d\rho_1 \int_0^1 \rho_2 d\rho_2 \int_0^{2\pi} K_0[kr_w \rho_{12}] d\theta; \quad \rho_{12} = [\rho_1^2 - 2\rho_1\rho_2 \cos\theta + \rho_2^2]^{1/2} \quad (36)$$

Using the representation ([18], Sec. 7.15)

$$\int_0^{2\pi} K_0[kr_w \rho_{12}] d\theta = 2\pi \begin{cases} K_0[kr_w \rho_1] I_0[kr_w \rho_2], & \rho_1 > \rho_2 \\ K_0[kr_w \rho_2] I_0[kr_w \rho_1], & \rho_1 < \rho_2 \end{cases} \quad (37)$$

and expansions of the functions K_0 and I_0 at small arguments,

$$K_0(z) \approx \ln\left(\frac{2}{z}\right) - \gamma_{Euler} + O(z^2 \ln z); \quad I_0(z) \approx 1 + O(z^2), \quad (38)$$

one finds that

$$\Lambda \approx \ln\left(\frac{2}{kr_w}\right) - \gamma_{Euler} + \frac{1}{4} + O(k^2 r_w^2 \ln kr_w) \quad (39)$$

where $\gamma_{Euler} = 0.5772$ is the Euler constant ([18], Sec. 1.1).

For the other distributions of the current over the cross-section of the wire, the term $1/4$ in (39) should be replaced by a form-factor F . In other words, in a more general case,

$$\Lambda \approx \ln\left(\frac{2}{kr_w}\right) - \gamma_{Euler} + F + O(k^2 r_w^2 \ln kr_w) \quad (39')$$

For the current flowing only over the surface of the wire (strong skin effect) $F=0$.

D. The accuracy of evaluating the force terms

Errors in evaluating force terms on the equations of motion are caused by the finiteness of the wire radii, r_w . These errors grow with the growth of the wave number. In our further analysis, we will restrict ourselves to the first three terms in the r.h.s. of Eq. (39'). The relative error in Λ is then of the order of $(kr_w)^2$. A 10% error would correspond to $kr_w \sim 0.3$. This means that, even for wires with $r_w/a \sim 0.25$, i.e., for the wires occupying a half of the interwire gap, a 10% accuracy can be guaranteed even for $ka=1$.

One more source of error stems from the effect of a finite wire radius on the force acting between neighboring wires. For example, the force acting between two neighboring wires of finite radius is larger by a factor $\left[1 + \alpha(r_w/a)^2\right]$ than the force acting between two wires of zero radius (α is a numerical factor depending on the current distribution over the cross-section, e.g., ~ 0.5 for uniform current). For $r_w/a \sim 0.25$ this error does not exceed $\sim 10\%$. So, we conclude that our predictions will have a quantitative meaning even for relatively thick wires, occupying a half of the inter-wire distance.

V. DISPERSION RELATIONS

A. General dispersion relations

Substituting expressions (27) and (30) into Eqs. (17)-(19), and taking into account Eqs. (1) and (5) one finds the following dispersion relations for the medial (M)

$$\hat{\gamma}^4 + F_M \hat{\gamma}^2 - \hat{k}^2 = 0 \quad (40)$$

and the lateral (L)

$$\hat{\gamma}^2 + F_L = 0 \quad (41)$$

modes. We have introduced the dimensionless growth rate,

$$\hat{\gamma} \equiv \gamma \sqrt{a/g}, \quad (42)$$

and the dimensionless wave number

$$\hat{k} \equiv ka \quad (43)$$

The functions F_M and F_L are:

$$F_M = -\frac{\hat{k}^2 \Lambda}{2\pi} + \frac{2\hat{k}^2}{\pi} \sum_{n=1}^{\infty} \cos\left(\frac{2\pi mn}{N}\right) K_1'(\hat{k}n) + \frac{\pi}{3} \quad (44)$$

$$F_L = -\frac{\hat{k}^2 \Lambda}{2\pi} + \frac{2\hat{k}}{\pi} \sum_{n=1}^{\infty} \cos\left(\frac{2\pi mn}{N}\right) \frac{K_1(\hat{k}n)}{n} - \frac{\pi}{3} \quad (45)$$

Equation (40) is a quadratic equation in $\hat{\gamma}^2$ and, therefore, for any given m , describes two modes; Eq. (41) describes one mode. As m runs from 0 to $N-1$, the total mode number (for a given k) is $3N$, as it should be. In other words, our solution covers *all* the possible modes in the set of thin wires.

As a curiosity, one can mention that the functions F for the medial and the lateral modes with the same value of m are related to each other by the following equation which is a consequence of Eqs. (44), (45), and (39'):

$$F_M = \hat{k}^2 \frac{\partial}{\partial \hat{k}} \left(\frac{F_L}{\hat{k}} \right) - \frac{\hat{k}^2}{2\pi} \quad (46)$$

The unstable solution of Eq. (40) is:

$$\gamma_M^2 = -\frac{F_M}{2} + \sqrt{\frac{F_M^2}{4} + \hat{k}^2} \quad (47)$$

At a given k , the maximum (over the azimuthal mode number m) growth rate corresponds to a minimum (over m) value of F_M . As is known from the theory of the Bessel functions, the derivative K_1' is universally negative. This, in turn, means that the maximum growth rate of a medial mode corresponds to $m=0$ (“axisymmetric” perturbation). As is clear from (41), for the lateral mode the maximum growth rate is also reached at a minimum of F_L . One can show that the minimum of F_L (the maximum growth rate) in this case corresponds to $m=N/2$, i.e., to the opposite displacements of the neighboring wires.

B. Asymptotic properties of the functions F_M and F_L

At large \hat{k} 's, $\hat{k} \gg 1$, the McDonald's functions are exponentially small, and so are the sums over n in the expressions (44) and (45). In addition, one can neglect the last term compared to the first term in each of these expressions. Therefore, we conclude that

$$F_L \approx F_M \approx -\frac{\hat{k}^2 \Lambda}{2\pi}, \quad \hat{k} \gg 1 \quad (48)$$

It goes without saying that we still assume that k is smaller than the inverse radius of an individual wire, i.e., $\hat{k} < a/r_w$. (for the numerical example given in the Introduction, the r.h.s. is ~ 60). To find the trends of the instability behavior with decreasing (although still large) \hat{k} 's, one can retain the last term in Eqs. (44) and (45), as well as the first ($n=1$) term.

in the sums over n (this term is proportional to $\exp(-\hat{k}n)$, while the next term is proportional to $\exp(-2\hat{k}n)$ and is, therefore, much smaller). In this improved approximation one finds that

$$F_M = -\frac{\hat{k}^2 \Lambda}{2\pi} + \frac{2\hat{k}^2}{\pi} \cos\left(\frac{2\pi m}{N}\right) K_1'(\hat{k}) + \frac{\pi}{3} \quad (48')$$

$$F_L = -\frac{\hat{k}^2 \Lambda}{2\pi} + \frac{2\hat{k}}{\pi} \cos\left(\frac{2\pi m}{N}\right) K_1(\hat{k}) - \frac{\pi}{3} \quad (48'')$$

These expressions should have an accuracy of $\sim 10\%$ at \hat{k} as low as 1 (because the next, $n=2$, term will be $\sim \exp(-2)$). Note that $K_1'(\hat{k}) < 0$, so that the sign of the second term in Eq. (48') is opposite to the sign of the cosine multiplier.

Consider now the case of small \hat{k} 's, $\hat{k} \ll 1$. The leading terms in the expansion of the McDonald's function at small values of the argument are:

$$K_1(z) = \frac{1}{z} + \frac{z}{2} \ln|z| + O(z); \quad zK_1'(z) = -\frac{1}{z} + \frac{z}{2} \ln|z| + O(z) \quad (49)$$

To the lowest order in \hat{k} one, therefore, finds:

$$F_L = -F_M = \frac{2}{\pi} \sum_{n=1}^{\infty} \frac{\cos(2\pi mn/N)}{n^2} - \frac{\pi}{3} \quad (50)$$

The sum in (50) can be found from the following identity:

$$\sum_{n=0}^{\infty} \frac{\cos zn}{n^2} = \frac{\pi^2}{6} - \frac{\pi|z|}{2} + \frac{z^2}{4}, \quad -\pi \leq z \leq \pi \quad (51)$$

(outside the interval $-\pi \leq z \leq \pi$ the sum can be found by a periodic continuation of the r.h.s.). At small m 's, when

$$\hat{q} \equiv \frac{2\pi m}{N} \ll 1 \quad (52)$$

the azimuthal dependence of the displacement becomes quasi-continuous (displacements of the neighboring wires are almost the same). In this case the quantity $q \equiv \hat{q}/a$ plays the role of azimuthal wave number.

One can show (see Appendix 1) that, at both \hat{k} and \hat{q} small, the following representations are valid:

$$F_L \approx \sqrt{\hat{k}^2 + \hat{q}^2}; F_M \approx -\frac{\hat{q}^2}{\sqrt{\hat{k}^2 + \hat{q}^2}} \quad (53)$$

C. Instability in some limiting cases

1. Kink instability of individual wires ($\hat{k} \gg 1$)

In the limit of $\hat{k} \gg 1$ (i.e., for the axial wave numbers greatly exceeding the inverse inter-wire distance), one can retain only the first term in the asymptotic expansions (48') and (48''). The dispersion relation for the medial mode predicts an instability with the growth rate

$$\hat{\gamma}_M \approx \gamma_{kink} \equiv \hat{k} \sqrt{\Lambda/2\pi} \quad (54)$$

This is a familiar kink instability of individual wires (see, e.g. [19]).

The lateral mode in this approximation has the same growth rate as the medial mode:

$$\hat{\gamma}_L \approx \gamma_{kink} \quad (55)$$

One sees that the two modes are in this approximation degenerate.

At large but finite values of \hat{k} 's, two new effects surface: first, degeneracy disappears. Second, interaction between the neighboring wires comes into play. This is signified by the appearance of the dependence of functions F_M and F_L on m . For the lateral mode, one finds:

$$\hat{\gamma}_L = \gamma_{kink} \sqrt{1 - \frac{4}{\Lambda \hat{k}} \cos \frac{2\pi m}{N} K_1(\hat{k}) + \frac{2\pi^2}{3\Lambda \hat{k}^2}} \quad (56)$$

(see (48'')). For $m=N/2$ which corresponds to opposite displacements of the neighboring wires (Fig. 3), the growth rate increases compared to the case where the interaction is neglected. A qualitative explanation of this fact is as follows: When two neighboring wires bend in the opposite direction (as it happens in the lateral mode $m=N/2$, Fig.3b) the attraction between the parts that are closer to each other increases, thereby causing the increase of the growth rate. For the other lateral modes (other m 's) the interaction between the wires gives a smaller increase in the growth rate (or even a decrease, as for the mode with $m=0$, Fig. 3a).

We will not write down a lengthy solution of Eq. (40) for the medial mode with F_M as in (48'). We just note that, for a given \hat{k} , the growth rate is bigger for the modes where the cosine multiplier in (48') is positive. Therefore, the growth rate for an antisymmetric mode ($m=N/2$) is smaller than for a symmetric mode ($m=0$) — opposite to the case of lateral modes.

2. Axisymmetric modes ($m=0$)

At $m=0$ and small k 's one can use expansion

$$\hat{k} \sum_{n=1}^{\infty} \frac{K_1(\hat{k}n)}{n} - \frac{\pi^2}{6} = -\frac{\pi |\hat{k}|}{2} \quad (57)$$

Therefore, at small k , the growth-rate of the $m=0$ medial mode is

$$\hat{\gamma}_M = \sqrt{\hat{k}} \quad (58)$$

In other words, we recover growth rate of the Rayleigh-Taylor instability of a continuous conducting shell (e.g., [5]). At larger \hat{k} 's approaching unity, F_M becomes non-zero, and the growth-rate increases compared to Eq. (58). At $\hat{k} > 1$, one can use Eq.(48') to evaluate F_M . In this domain, the growth rate is determined by Eq. (47) with $m=0$.

An axisymmetric L-mode can be called a “zonal flow mode” mode (Fig. 6b), by analogy with the patterns of atmospheric circulation forming rings of eastward or westward flow. Its growth rate at small k 's is, according to (57),

$$\hat{\gamma}_L = \sqrt{\hat{k}} \quad (59)$$

At higher k 's, one can use Eq. (56). This mode is of interest in that it causes a twisting of the array and may serve as a source of spontaneously excited zonal flows (azimuthal flows with directions alternating along the axis). In the course of the implosion, these zonal flows may be enhanced by virtue of the conservation of the angular momentum.

3. Perturbations without axial dependence

We emphasize that we cannot just put $\hat{k}=0$, because then we would have to take into account the possibility of the current variation in the wires. This latter case was considered by Samokhin [10]. As for this paper, we simply assume that the axial wavelength is much less than the azimuthal wavelength.

At $\hat{k} \rightarrow 0$, according to Eqs. (40), (50), and (51), the medial modes are stable, whereas the lateral modes are unstable. Therefore, we concentrate on the latter. Consider, first, the modes of highest symmetry, $m/N=1/2$. For these modes the neighboring wires experience displacements in the opposite directions (Fig.3). It is clear from Eq. (11) that

$m/N=1/2$ correspond to $z=\pi$. Then, Eqs. (49) and (51) yield $F_M = -F_L = \pi/2$. The growth rate for the lateral mode is (the medial mode is stable):

$$\hat{\gamma}_L^{(1/2)} = \sqrt{\pi/2} \quad (60)$$

The superscript “1/2” signifies the fact that $m/N=1/2$. The mode can be called a “coalescence” mode, because it corresponds to coalescence of pairs of wires. It is clear from the discussion of Sec. III.A and Eq. (51) that the $m/N=1/2$ mode has maximum possible growth rate among the $\hat{k} \rightarrow 0$ modes.

4. Perturbations with small wave numbers ($\hat{k}, \hat{q} \ll 1$)

Consider now waves with small azimuthal mode numbers (small m/N). Displacements of the neighboring wires in this case differ only by a small amount (see Eq. (11)) and the mode becomes quasicontinuous (Fig. 3d). It can be characterized by the azimuthal wave number (51). The y dependence of the displacement is proportional to $\exp(iqy)$. The dimensionless mode number is $\hat{q} \equiv qa$. At small k and q , one can use expressions (53) for F_L and F_M . This gives rise to the following dispersion relations:

$$\hat{\gamma}^4 + \frac{\hat{q}^2}{\sqrt{\hat{k}^2 + \hat{q}^2}} \hat{\gamma}^2 - \hat{k}^2 = 0 \quad (M\text{-mode}) \quad (61)$$

$$\hat{\gamma}^2 - \sqrt{\hat{k}^2 + \hat{q}^2} = 0 \quad (L\text{-mode}) \quad (62)$$

The long-wavelength lateral mode is universally unstable. Note that the lateral mode was absent in the model of a perfectly conducting continuous shell [5]. The reason for this difference is a strong anisotropy of the electrical conductivity of the wire array (considered from a macroscopic point of view): there is an infinite conductivity along the wires, but zero conductivity across the wires (in the y direction in the unperturbed state).

The anisotropy of the conductivity is significant also for the medial mode: in the approximation $\hat{k} \rightarrow 0$ the medial mode is stable. This result is in sharp contrast with the case of a perfectly conducting thin shell, where the growth rate for the modes with $k \ll q$ is (e.g., [5]):

$$\sqrt{|\hat{q}|(\sqrt{2}-1)}. \quad (63)$$

The difference with the model of a perfectly conducting shell is caused, again, by the anisotropy of the electrical conductivity.

For long-wavelength modes the presence of the return current conductor may become non-negligible. However, analysis shows that, in practical terms, these effects are usually sub-dominant. The reason is that the image currents are situated at a distance $2D$ from the wire array, and perturbations produced by image current in the location of the wire array contain a multiplier $\exp(-2kD)$. This factor becomes non-negligible at, roughly speaking $2kD \sim 1$, i.e., at the axial wavelength $\lambda \sim 4\pi D$. Even for unrealistically small value of $D \sim 1$ mm, λ exceeds 1 cm. Such wavelengths are usually of little concern in the stability of wire array implosions, where perturbations with $\lambda \sim 1-3$ mm dominate.

Note also that the presence of the image currents causes a mixing of the medial and lateral modes: for a tightly fit return current conductor these modes are coupled.

D. Numerical results

The dispersion relations contained in Eq.(40) and Eq.(41) can be evaluated numerically for a range of values of \hat{k} , m/N , and r_w/a . The normalized growth rates for the lateral (dashed curves) and medial modes (solid curves) are plotted in Fig. 6, as a function of \hat{k} , for fixed values of m/N and r_w/a . The growth rate of the classical Rayleigh-

Taylor mode, $\gamma = k^{1/2}$, is plotted for reference (dotted curves). The asymptotic limits discussed in Section VC for large or small \hat{k} are evident, with the transition occurring near $\hat{k} \sim 1$. The curves are terminated at $\hat{k} r_w / a = 1$, where the small wire approximation becomes marginal.

Fig.7 shows the normalized growth rates for the lateral (dashed curves) and medial modes (solid curves) as a function of m/N , for fixed $\hat{k}=2$ and $r_w/a = 0.1$. The classical Rayleigh-Taylor mode growth rate, for reference, is shown as a dotted line. As discussed in Section VC, the medial mode growth rate is maximized at $m/N=0$ and the lateral mode growth rate is maximized at $m/N = 0.5$. From inspection of Fig. 6, we see that lateral modes with $m/N = 0.5$ grow faster than medial modes with $m/N = 0$ at small values of \hat{k} , while medial modes with $m/N = 0$ are dominant at large \hat{k} . The critical value of \hat{k} , above which the growth rate of the fastest growing medial mode ($m/N = 0$.) exceeds the growth rate of the fastest growing lateral mode ($m/N = 0.5$), is plotted in Fig. 8 as a function of a/r_w .

V DISCUSSION

We have presented a complete classification of the eigenmodes of a wire array in a thin-wire approximation. Equations (40)-(45) provide the way for evaluating the growth rate of any linear mode. It turns out that this approximation has a reasonable accuracy even if the ratio of the wire radius to the inter-wire distance is not very small, ~ 0.25 . In agreement with the previous analysis of Felber and Rostoker, we have found that there are two uncoupled groups of modes, the medial modes, in which the wires experience displacements in the r - z (x - z) plane, and the lateral modes, in which displacements have only an azimuthal component.

It turns out that considerable deviation from the scaling $\gamma \sim k^{1/2}$ occurs only at large wave numbers, greater than ~ 2 inverse interwire spacings and for very small wire radius, $a/r_w > 20$. Only here kink modes characteristic of the instability of individual wires become dominant. For azimuthally symmetric modes ($m=0$), the growth rate at $ka \sim 1$ is rather close to the $(kg)^{1/2}$. For realistic conditions of wire array experiments at Sandia National Laboratory with ~ 200 tungsten wires, we expect $a/r_w \sim 10$ or less due to early-time explosion of the wires before MHD forces become significant. Still, 20-30% increase over $(kg)^{1/2}$ is possible. This may be important in the interpretation of the observed in [20] dependence of the implosion quality on the number of wires in the array (Desjarlais and Marder, [21]). Interestingly enough, the lateral modes at $ka \sim 1$ have a growth rate not very different from medial modes.

The modes with small wave numbers probe the average, macroscopic properties of the array, specifically, the anisotropy of its conductivity. Because of this anisotropy, they have properties very different from the properties of the modes of a thin perfectly conducting shell: in the case of a wire array, there appears a new, lateral, mode of a zonal flow type, which is strongly unstable; on the other hand, the medial modes become more stable. In principle, this observation can be used for diagnosing the presence of the anisotropy of conductivity: one can, for instance, create large enough perturbations of the medial type and follow their evolution during the first phase of the implosion. Until the inter-wire conductivity becomes large, they should remain stable.

Hot halo plasma formed early in the pulse can provide electrical contact between the neighboring wires. There are two mechanisms which, in fact, may cause a significant delay in the occurrence of interwire currents. The first is related to the effect of “blowing” this low-density plasma through the array towards the axis. The second is also related to the low density of this plasma: even if it is in electric contact with the cores of neighboring wires, when the currents through it start flowing, their interaction with the magnetic field leads to very fast displacements of this halo towards a kind of a force-free configuration, in

which the current between the wires will be strongly suppressed. As these processes may be intimately linked with the overall performance of the wire array, an objective experimental assessment of the short-circuiting process seems important. In this sense, our analysis provides a reliable reference point.

ACKNOWLEDGMENT

The authors are grateful to J. DeGroot, M. Desjarlais, B. Marder, M.K. Matzen, R. Spielman, and A. Toor for useful discussions and general interest in this work. This work was carried out under the auspices of the U.S. Department of Energy by Lawrence Livermore National Laboratory under Contract W-7405-ENG-48. The work of D.D.R. was supported by Sandia National Laboratories.

Appendix. Instability in the limit of a quasi-continuous shell

In this Appendix, we present a derivation of dispersion relations in a long-wavelength limit. We represent the array as a continuous shell of infinitesimal thickness. Its deformation is characterized by a Lagrangian displacement vector $\xi(x,y)$ in the same fashion as in a thin-shell analysis by Ott [22] (who considered a pressure-driven acceleration of the shell, so that the conductivity issues were of no importance). The current flows along the lines into which initial straight lines parallel to the axis z are mapped.

Denoting by Δm the mass of a certain surface element of the initial surface area ΔS , one can write down the following equation for the perturbations:

$$\begin{aligned}\Delta m \ddot{\xi}_x &= -\delta J_z B_{yret} \Delta S - J_z \overline{\delta B}_y \Delta S - \delta J_z B_{yret} \delta \Delta S \\ \Delta m \ddot{\xi}_y &= J_z \overline{\delta B}_x \Delta S \\ \Delta m \ddot{\xi}_z &= -\delta J_x B_{yret} \Delta S\end{aligned}\tag{A.1}$$

where B_{yret} is the magnetic field (2) created by a return current conductor at the location of the array, $\overline{\delta B}_{x,y}$ is the perturbation of the magnetic field at $x=0$ (we will explain the meaning of the averaging bar shortly), and $J_z \equiv J$ is a surface current density (i.e., the current density integrated over the shell thickness) and $\delta J_{x,z}$ are its perturbations. The quantity $\delta \Delta S$ is a change of the surface area caused by the deformation of the shell:

$$\delta\Delta S = \Delta S \left(\frac{\partial \xi_y}{\partial y} + \frac{\partial \xi_z}{\partial z} \right) \quad (\text{A.2})$$

The bar over the magnetic field perturbation refers to the fact that the presence of the surface current in our problem, generally speaking, causes the appearance of discontinuities of the magnetic field at the surface of the shell. The bar means taking a half-sum of the values of the perturbation at the two sides of the current sheet (only this part of the perturbation gives rise to a net force acting at the surface current).

By noting that

$$-J_z B_{yret} = \frac{\Delta m}{\Delta S} g, \quad \delta J_z = -J_z \frac{\partial \xi_y}{\partial y}, \quad (\text{A.3})$$

and assuming the $\exp(\gamma + ikz + iqy)$ form of the perturbations, one finds:

$$\gamma^2 \xi_x = -g \frac{\overline{\delta B}_y}{B_{yret}} + ikg \xi_z; \quad \gamma^2 \xi_y = g \frac{\overline{\delta B}_x}{B_{yret}}; \quad \gamma^2 \xi_z = -ikg \xi_x \quad (\text{A.4})$$

To find the magnetic field perturbations, we use equations

$$\nabla \times \delta \mathbf{B} = \mu_0 \delta \mathbf{j} \quad (\text{A.5})$$

$$\nabla \cdot \delta \mathbf{B} = 0 \quad (\text{A.6})$$

The perturbation of the current density is:

$$\begin{aligned} \delta j_x &= ikJ\delta(x)\xi_x; \\ \delta j_y &= ikJ\delta(x)\xi_y; \end{aligned} \quad (\text{A.7})$$

$$\delta j_z = -J \frac{\partial \delta(x)}{\partial x} \xi_x - J\delta(x)iq\xi_y$$

Using x and y components of Eq. (A.5), together with Eq. (A.6), one arrives at the following equation for δB_z :

$$\delta B_z'' - (k^2 + q^2)\delta B_z = -\mu_0(\delta j_y' + iq\delta j_x) \quad (\text{A.8})$$

where primes denote the differentiation over x . The perturbation of the current is localized at the $x=0$ plane; therefore, one has basically to solve a homogeneous version of the Eq.

(A.8) in the half-spaces $x>0$ and $x<0$ and connect them via boundary conditions that follow from integrating Eq. (A.8) over the infinitesimally thin layer of the current sheath. The boundary conditions read:

$$\begin{aligned}\delta B_z' \Big|_{x=+0} - \delta B_z' \Big|_{x=-0} &= \mu_0 k q J \xi_x; \\ \delta B_z \Big|_{x=+0} - \delta B_z \Big|_{x=-0} &= -\mu_0 i k J \xi_x.\end{aligned}\tag{A.9}$$

We first present solution of the problem for $kD>1$, when one can neglect the presence of the return current conductor. In this case, one has to impose conditions that perturbations of the magnetic field vanish at large distances from the sheath. After finding δB_z and using the x and y components of Eq. (A.5) to express the other two components of the perturbation, one arrives at the following result:

$$\overline{\delta B}_x = \frac{\mu_0}{2} \sqrt{k^2 + q^2} J \xi_y \tag{A.10}$$

$$\overline{\delta B}_y = -\frac{\mu_0}{2} \frac{q^2}{\sqrt{k^2 + q^2}} J \xi_x \tag{A.11}$$

When substituted into (A.4), these equations immediately yield expressions (53) and dispersion relations (62) and (63). Note that one could limit oneself to evaluating only δB_x , (or, equivalently, of F_L) and then using relationship (46) in the limit of a small wave-numbers to derive F_M .

If the return current conductor is situated so close to the shell that $kD<1$, one has to take its presence into account. What changes in our analysis, is that now one has to impose a boundary condition

$$\delta B_z' \Big|_{x=-D} = 0 \tag{A.12}$$

This leads to a mixing between the medial and the lateral modes:

$$\begin{aligned}
\delta\bar{B}_x &= \frac{\mu_0}{2} \sqrt{k^2 + q^2} J\xi_y \left[1 - \exp\left(-2\sqrt{k^2 + q^2} D\right) \right] + \frac{\mu_0}{2} iqJ\xi_x \exp\left(-2\sqrt{k^2 + q^2} D\right) \\
\delta\bar{B}_y &= \frac{\mu_0}{2} \frac{q^2}{\sqrt{k^2 + q^2}} J\xi_x \left[1 + \exp\left(-2\sqrt{k^2 + q^2} D\right) \right] + \frac{\mu_0}{2} iqJ\xi_y \exp\left(-2\sqrt{k^2 + q^2} D\right)
\end{aligned} \tag{A.13}$$

The mixing reflects itself in that ξ_y now enters equation (A.4), and ξ_x enters the second of these equations. The mixing vanishes in the case $q=0$, in which case we find the medial mode growth rate is unaffected by the return conductor, $\gamma = \sqrt{kg}$. However, the $q=0$ lateral, zonal-flow type mode is partially stabilized by the presence of the conductor. Making use of (A.13) in (A.4), we find $\gamma = \sqrt{kg(1 - \exp(-2kD))}$. We will not go further in the analysis of the perturbations in this case.

Figure captions.

Fig. 1. The geometry of the problem: (a) The cylindrical wire array 1 enclosed within the return current conductor 2 (only part of the latter is shown). The current along the wires (shown are six wires at the front part of the array) is directed upward. The usual relationship between a , D , and r is: $a \ll D \ll r$. This allows one to substitute a planar analog for the real system. (b) The planar analog. The unperturbed magnetic field is localized between the wire array and return-current conductor.

Fig. 2. Lagrangian description of the perturbation of an individual wire.

Fig. 3 A few lateral perturbations: $m=0$ (a); $m=N/2$ (b); $m=N/4$ (c); $m=N/10$ (d).

Fig. 4. Representation of the current perturbation by a sequence of infinitesimal current loops (magnetic dipoles). Shown are two loops, 1 and 2. The currents in the adjacent elements of these loops cancel each other.

Fig. 5. Cross-sections of two current filaments by the plane $z=0$; the total current is a sum over such filaments.

Fig. 6. The normalized growth rates for the medial (solid curves) and lateral (dashed curves) modes as a function of the normalized wave number \hat{k} for $m/N=0$ and $m/N=1/2$. The growth rate for a classical Rayleigh-Taylor mode $\hat{\gamma} = \hat{k}^{1/2}$ is plotted for reference (dotted line).

Fig. 7. The normalized growth rates for the medial (solid curve) and lateral (dashed curve) modes as a function of m/N , for $\hat{k}=2$ and $r_w/a=0.1$. The growth rate for a classical Rayleigh-Taylor mode is plotted for reference (dotted line).

Fig. 8. The critical value of \hat{k} vs. the parameter a/r_w . For \hat{k} values above the curve, the fastest growing mode is the medial mode with $m/N=0$; below the curve, the fastest growing mode is the lateral mode with $m/N=1/2$.

References

1. M.K. Matzen. Phys. Plasmas, **4**, 1519, (1997).
2. R.B. Spielman, C. Deeney, G.A. Chandler, M.R. Douglas, D.L. Fehl, M.K. Matzen, D.H. McDaniel, T.J. Nash, J.L. Porter, T.W.L. Sanford, J.F. Seamen, W.A. Stygar, K.W. Struve, S.P. Breeze, J.S. McGurn, J.A. Torres, D.M. Zagar, T.L. Gilliland, D.O. Jobe, J.L. McKenney, R.C. Mock, M. Vargas, T. Wagoner, D.L. Peterson, Phys. Plasmas, **5**, pt.2, 2105 (1998).
3. T.W.L Sanford, T.J. Nash, R.C. Mock, R.B.Spielman, K.W.Struve, J.H. Hammer, J.S. DeGroot, K.G. Whitney, J.P. Apruzese, Phys. Plasmas, **4**, 2188 (1997).
4. S. Chandrasekhar. *"Hydrodynamic and hydromagnetic stability."* Clarendon Press 1961.
5. E.G. Harris. Phys. Fluids, **5**, 1057 (1962).
6. J.H. Hammer, J.L. Eddleman, P.T. Springer, M. Tabak, A. Toor, C. Deeney, R. Humphries, T.J. Nash, T.W.L. Sanford, R.B. Spielman, J.S. DeGroot. Phys. Plasmas, **3**, 2063 (1996).
7. A.L. Velikovich, J. Davis. Phys. Plasmas, **2**, 4513 (1995).
8. D.L. Peterson, R.L. Bowers, J.H. Brownell, C. Lund, W. Matuska, K. McLenithan, H. Oona, C. Deeney, M. Derzon, R.B. Spielman, T.J. Nash, G. Chandler, R.C.

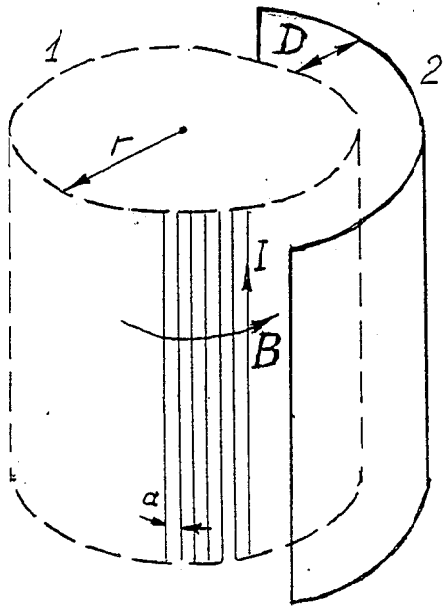
- Mock, T.W. L. Sanford, M.K. Matzen, N. Roderick. In: "Dense Z-pinches," AIP Conference Proceedings, v. 409. p. 201 (1997).
9. F.S. Felber, N. Rostoker. Phys. Fluids, **24**, 1049 (1981).
10. A.A. Samokhin. Journ. Appl. Mech. Techn. Phys., **28**, 89 (1988).
11. J. DeGroot. Private communication.
12. L.E. Aranchuk, S.L. Bogolyubskii, G.S. Volkov, V.D. Korolev, Yu.V. Koba, V.I. Liksonov, A.A. Lukin, L.B. Nikandrov, O.V. Tel'kovskaya, M.V. Tulupov, A.S. Chernenko, V.Ya. Tsarfin, V.V. Yan'kov. Sov. J. Plasma Phys., **12**, 765 (1986).
13. D. Kalantar, D. Hammer. Phys. Rev. Lett., **71**, 3806 (1993).
14. F.N. Beg, A. E. Dangor, P. Lee, M. Tatarakis, S.L. Niffikeer, M.G. Haines. Plasma Phys. Contr. Fusion. **39**, 1 (1997).
15. D. Reisman, Private communication.
16. L.D. Landau, E.M.Lifshitz. "*Statistical Physics.*" NY, Pergamon Press, 1980.
17. L.D. Landau, E.M.Lifshitz. "*Classical Theory of Field.*" NY, Pergamon Press, 1979.
18. H. Bateman, A. Erdelyi. "*Higher Transcendental Functions.*" McGraw-Hill Book Company, Inc., NY-Toronto-London, 1953.

19. J.P. Freidberg. *Rev. Mod. Phys.*, **54**, 801 (1981).

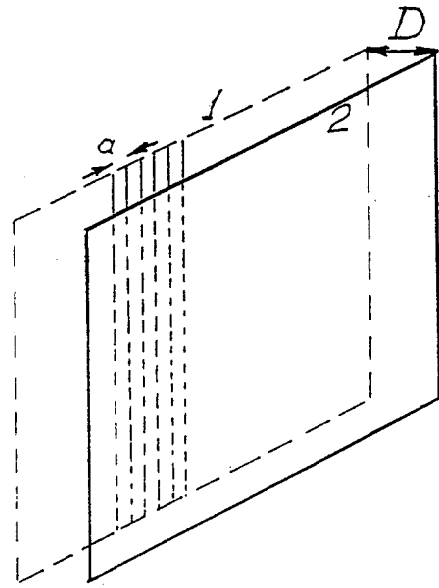
20. Sanford, T.W.L., G.O. Allhouse, B.M. Marder, R.C. Mock, R.B. Spielman, J.F. Seamen, J.C. McGurn, D. Jobe, T.L. Gilliland, M. Vargas, K.W. Struve, W.A. Stygar, M.R. Douglas, M.K. Matzen, J.H. Hammer, J.S. DeGroot, J.L. Eddleman, D.L. Peterson, D. Mosher, K.G. Whitney, J.W. Thornhill, P.E. Pulsifer, J.P. Apruzese, Y. Maron, *Phys. Rev. Lett.*, **77**, 5063 (1996).

21. M. Desjarlais and B. Marder, Private communication.

22. E. Ott. *Phys. Rev. Lett.* **29**, 1429 (1972).



(a)



(b)

Fig. 1

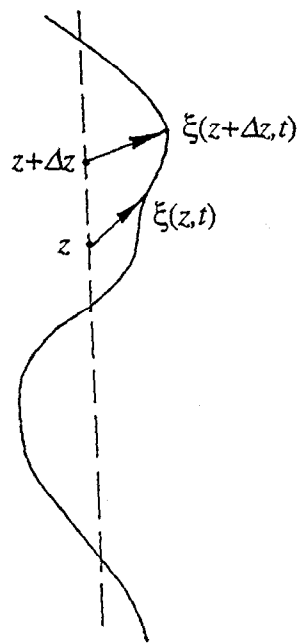


Fig. 2

Lateral mode structure for $m/N_{\text{wire}} = 1.000$

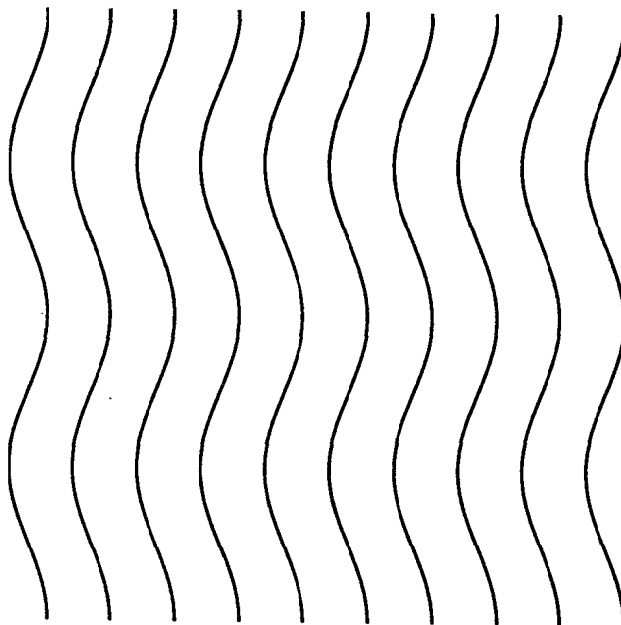


Fig. 3a

Lateral mode structure for $m/N_{\text{wire}} = 0.500$

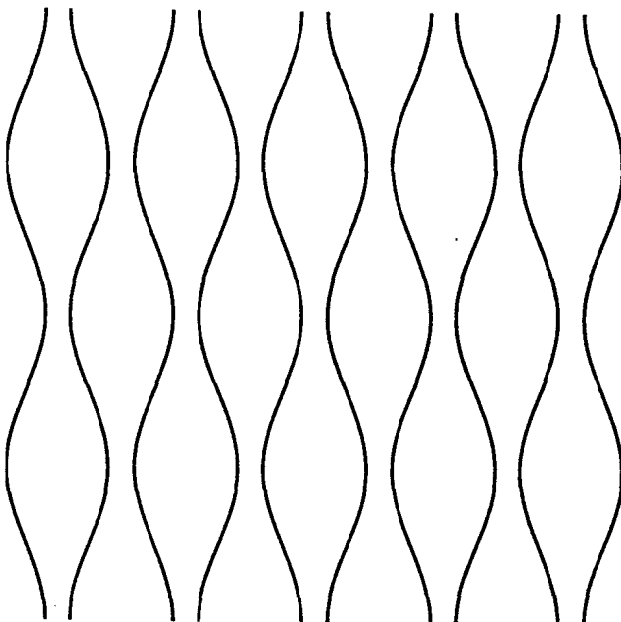


Fig. 3b

Lateral mode structure for $m/N_{\text{wire}} = 0.250$

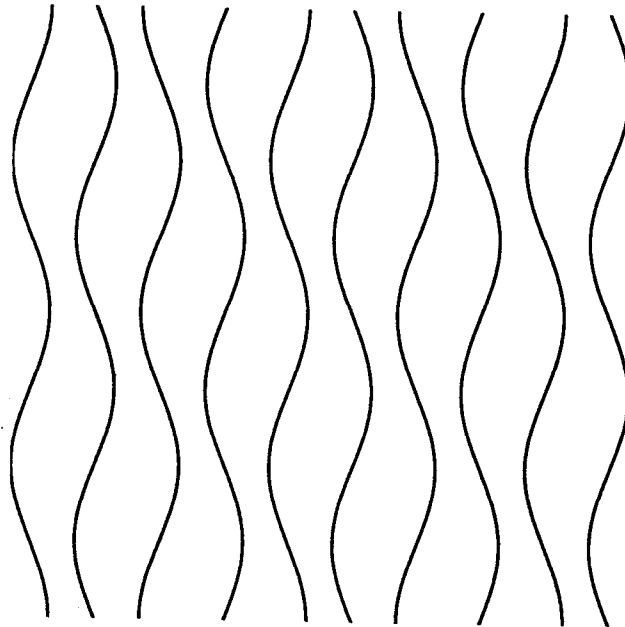


Fig. 3c

Lateral mode structure for $m/N_{\text{wire}} = 0.100$

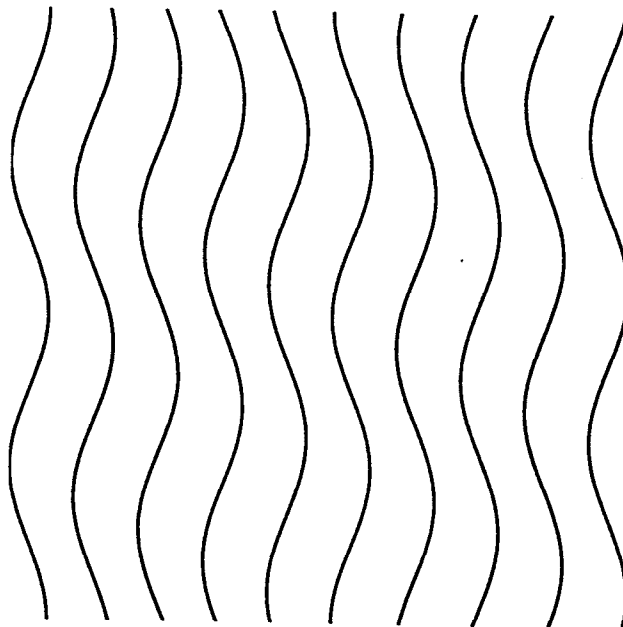


Fig. 3d

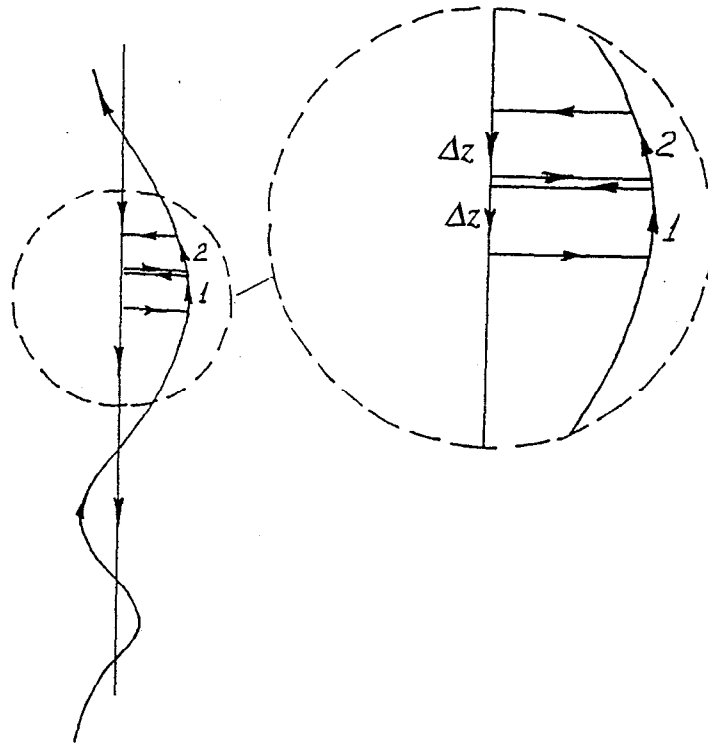


Fig 4

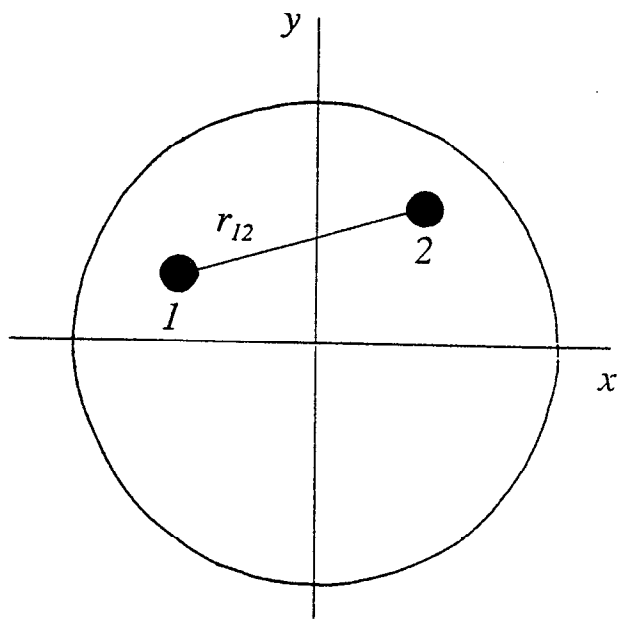
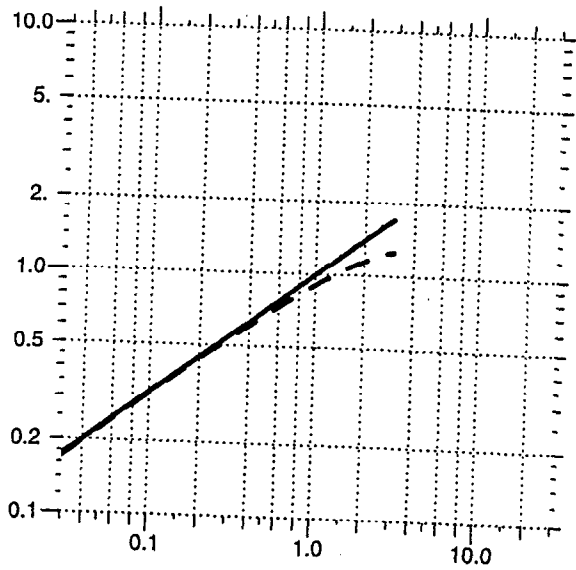
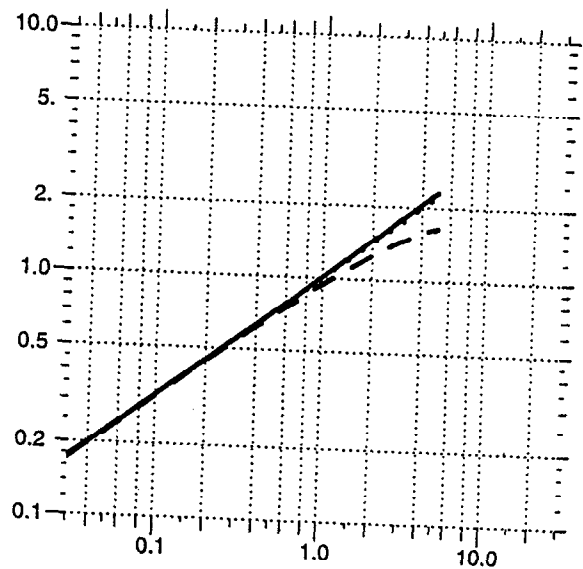


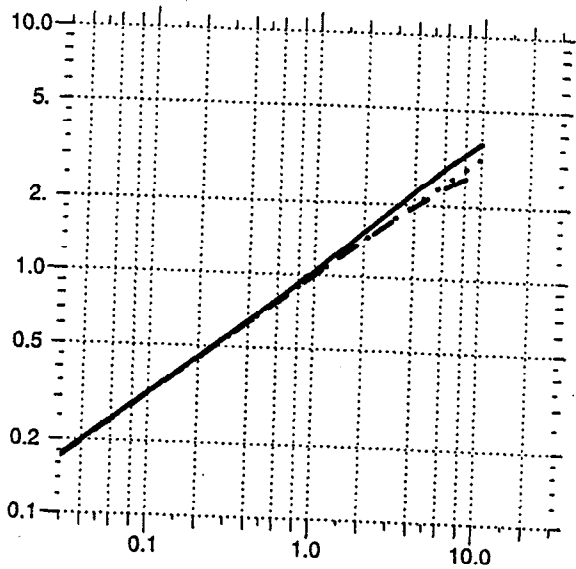
Fig. 5



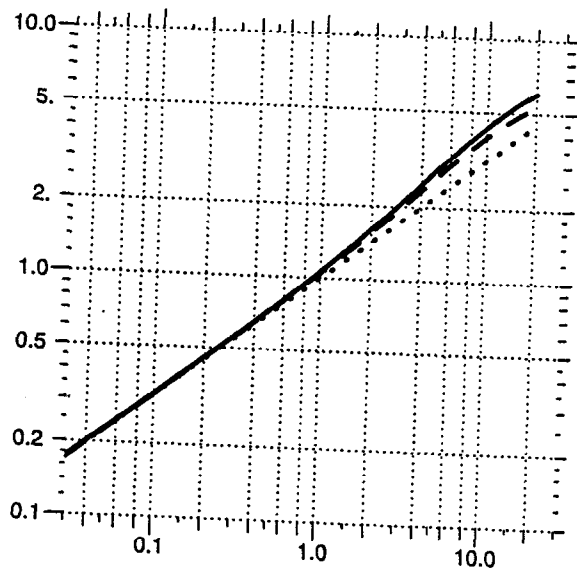
$a/r_{\text{wire}} = 3. \quad m/N = 0.$



$a/r_{\text{wire}} = 5. \quad m/N = 0.$

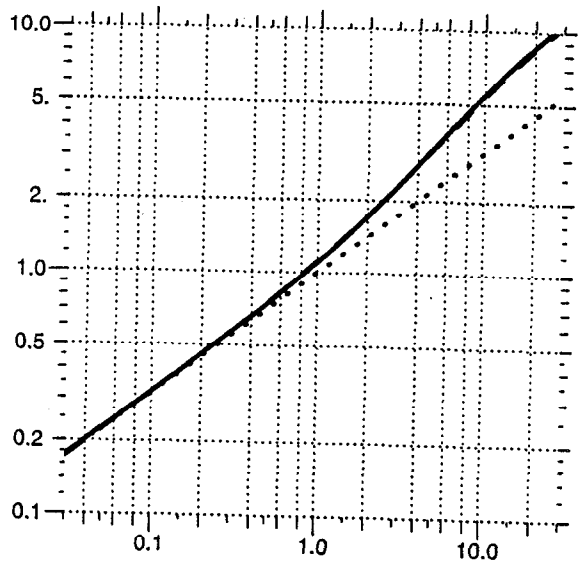


$a/r_{\text{wire}} = 10. \quad m/N = 0.$

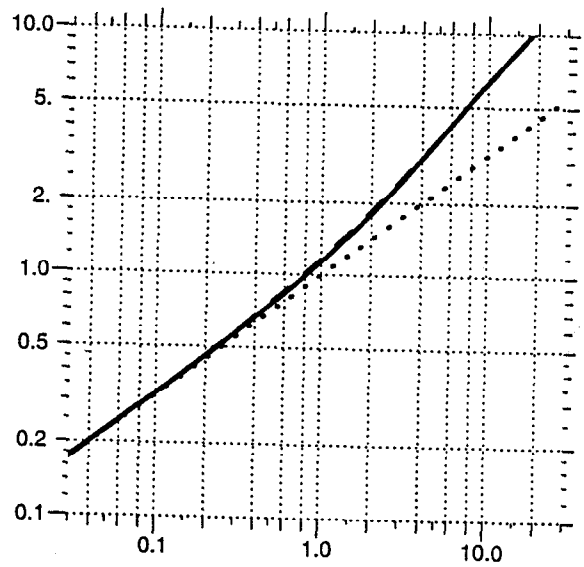


$a/r_{\text{wire}} = 20. \quad m/N = 0.$

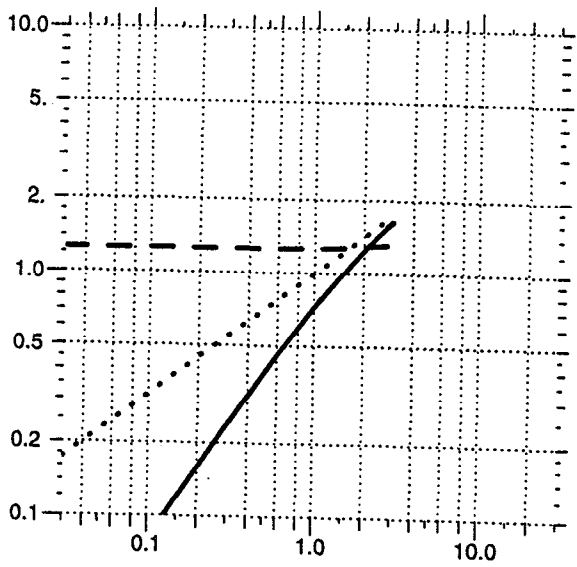
Fig 6 a-d



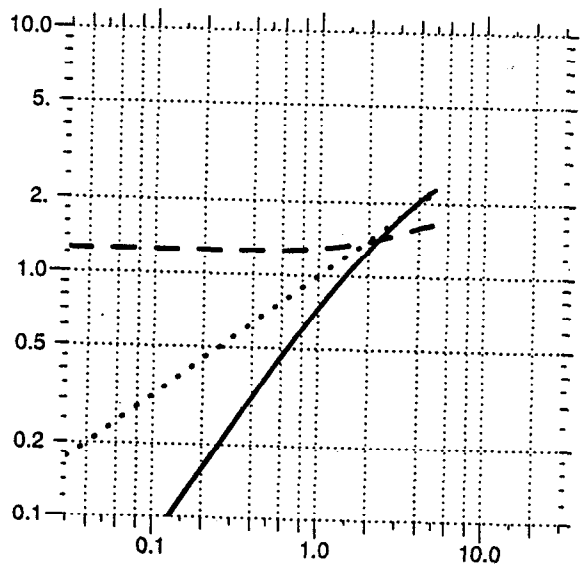
$a/r_{\text{wire}} = 50. \quad m/N = 0.$



$a/r_{\text{wire}} = 100. \quad m/N = 0.$

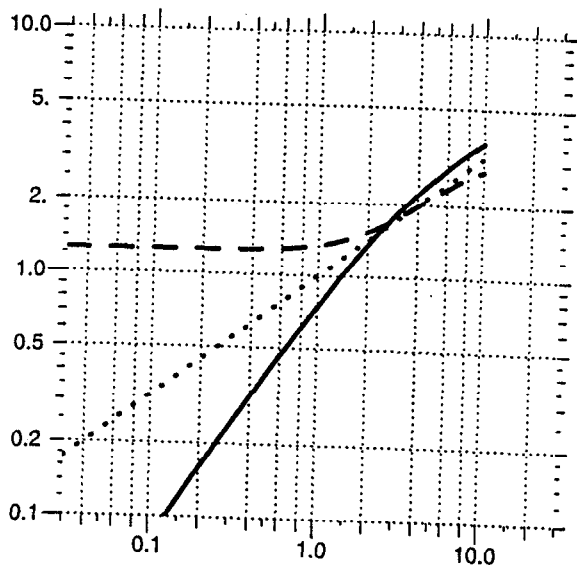


$a/r_{\text{wire}} = 3. \quad m/N = 0.5$

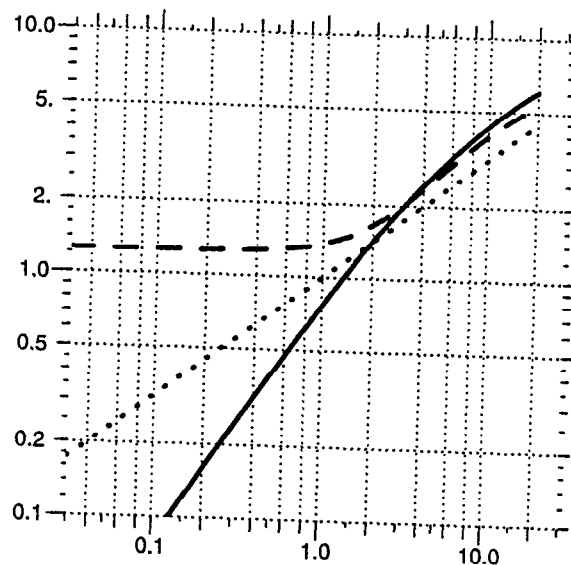


$a/r_{\text{wire}} = 5. \quad m/N = 0.5$

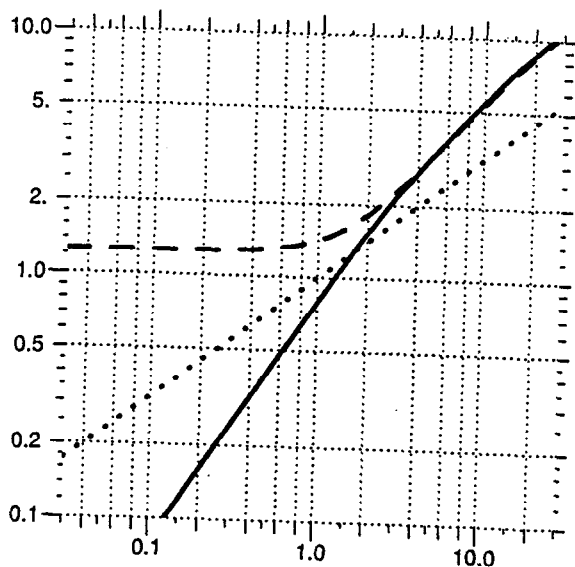
Fig6 e-h



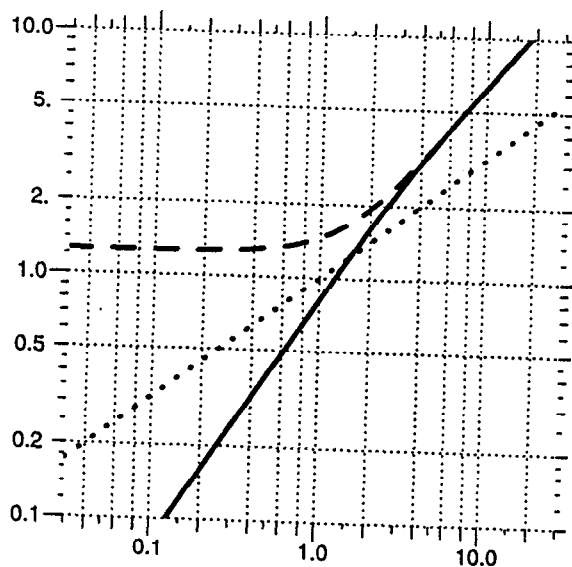
$a/r_{\text{wire}} = 10. \quad m/N = 0.5$



$a/r_{\text{wire}} = 20. \quad m/N = 0.5$



$a/r_{\text{wire}} = 50. \quad m/N = 0.5$



$a/r_{\text{wire}} = 100. \quad m/N = 0.5$

Fig 6 i-1

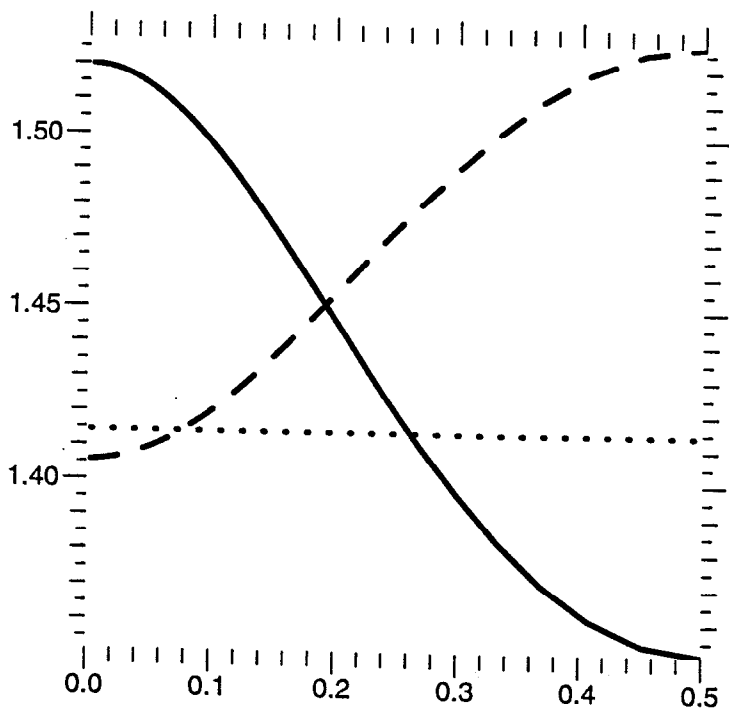


Fig. 7

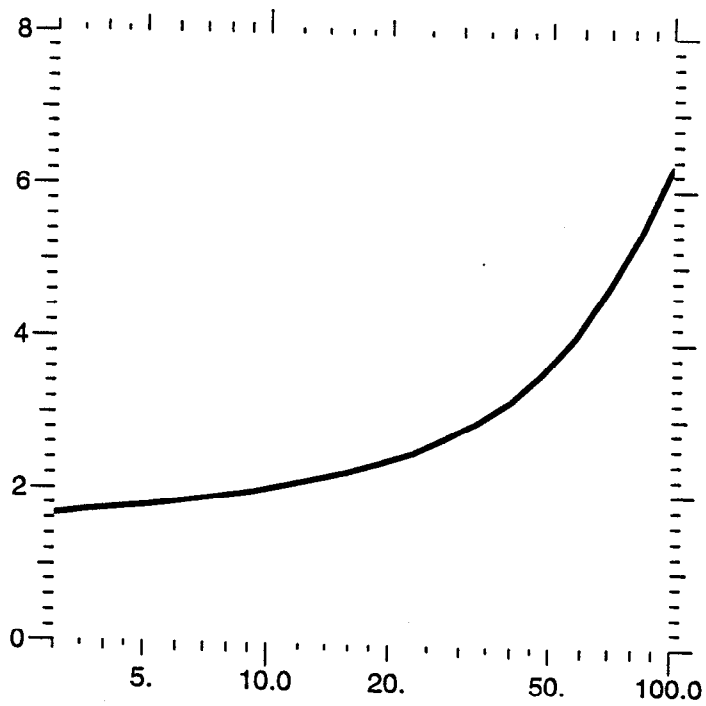


Fig. 8

